Volume 22, No 2 | International Journal of Radiation Research, April 2024

Diagnostic efficacy of combined fractional anisotropy and mean kurtosis in detecting Parkinson disease in a model rat

Y. Chen[1], D. An[1], Y. Dong[2*]

[1]Department of Magnetic Resonance Imaging, First Hospital of Qinhuangdao, No. 258 Wenhua Road, Qinhuangdao, Hebei Province, PR China

[2]Department of Interventional treatment, First Hospital of Qinhuangdao, No. 258 Wenhua Road, Qinhuangdao, Hebei Province, PR China

► ***Original article***

Corresponding author:
Yanchao Dong, M.D.,
E-mail:
dyc_hometown@aliyun.com

Received: April 2023
Final revised: October 2023
Accepted: November 2023

Int. J. Radiat. Res., April 2024; 22(2): 339-345

DOI: 10.61186/ijrr.22.2.339

Keywords: *Fractional anisotropy, mean kurtosis, diffusion kurtosis imaging, Parkinson's disease.*

ABSTRACT

Background: Both fractional anisotropy (FA) and mean kurtosis (MK) in diffusion kurtosis imaging (DKI) have value in the diagnosis of Parkinson's disease (PD). We here investigated the sensitivity and specificity of FA and MK to explore which of these methods were more efficient in the early diagnosis of the PD rat model. ***Materials and Methods:*** Twenty male SD rats were injected with 6-OHDA into the right substantia nigra (SN) for modeling, and other 20 rats were included in control group. DKI was performed 5 weeks after modeling. The FA and MK values of the right SN were measured and analyzed. Receiver operating characteristic curve was used to evaluate the sensitivity and specificity of the above two value in the identifying PD. Immunohistochemistry of tyrosine hydroxylase (TH), Tunel assay, and Nissl staining in the SN was performed. ***Results:*** The FA, MK and FA+MK values in the PD group obtained on the 5th week were statistically significantly different from those of the control group ($P < 0.01$). The optimal cut-off FA+MK value (with respective area under the curve, sensitivity, specificity) was 1.404 (0.925, 95%, 75%), the Youden's index of FA+MK was higher than of either of the two alone. The FA, MK and FA+MK values correlated positively with the Tunel staining, while they correlated negatively with the TH and Nissl staining. ***Conclusions:*** At the 5th week, the diagnostic efficiency of the combined FA and MK values was better than of either of the two alone in diagnosing PD.

INTRODUCTION

Parkinson's disease (PD) is a progressive neurodegenerative disease that affects more than 7 million people worldwide [1]. With a rapidly aging population, the incidence rate of PD has gradually increased, and the disease has developed into a common disease that threatens the physical and mental health of the elderly [2]. Drug replacement therapy is used for PD treatment, however, it cannot prevent the development of the disease before its onset, which may produce more adverse reactions[3]. Studies have shown that the pathological process of PD is manifested by prodromal non-motor symptoms, such as rapid eye movement, sleep disturbance, olfactory and gastrointestinal dysfunction, which appear decades before the onset of motor symptoms [4]. However, since the onset of non-motor symptoms is much earlier than that of motor symptoms, the corresponding treatment before the onset of exercise symptoms may delay the onset of PD. Some studies have shown that the treatment can be achieved by inducing astrocytes to transform into neurons that produce the neurotransmitter dopamine [5]. Therefore, there is an urgent need to develop a non-invasive biomarker for the early diagnosis of PD to identify patients who have non-motor symptoms. This should also allow better outcomes with neuroprotective therapy. Neuroimaging methods may become a suitable tool to address this unmet medical need [6].

Several neuroimaging methods may become sensitive and specific for identifying markers that can be used for PD diagnosis, including some positron emission tomography (PET), and single-photon emission tomography (SPECT) ligands, such as ^{18}F-FDG, ^{11}C-raclopride, (^{11}C-CFT)-DAT, ^{11}C-PK11195, ^{18}F-FP-CIT PET, ^{99m}Tc-TRODAT-1 SPECT [7-11]. However, because of its high price and poor repeatability, it is difficult to evaluate the therapeutic effect of PD as a routine follow-up technique [11]. Magnetic resonance imaging (MRI) is favored by clinicians because of its high soft tissue resolution, moderate price and strong repeatability [12]. Specific MRI approaches such as susceptibility weighted MRI (SWI) or neuromelanin sensitive MRI (NM-MRI) evaluating brain iron accumulation have been described [5,13]. Structural connectivity and functional MRI have also been studied in this regard [14,15]. However, the results are inconclusive, and there is no

[DOI: 10.61186/ijrr.22.2.339]

existing consensus on specific methods and analysis.

Degenerative pathological changes in PD (e.g α-syn accumulation, neuronal loss and glial cell proliferation) may affect the diffusion characteristics of water molecules in the tissue microenvironment and lead to microstructure changes [16-18], which can be detected using diffusion-weighted MRI [6]. At present, diffusion tensor imaging (DTI) is a widely used diffusion-weighted MRI technique for observing the microstructure of neurodegenerative diseases [19]. DTI parameters, such as fractional anisotropy (FA) and mean diffusivity (MD), quantify the direction distribution of random motion of water molecules and the amplitude of rotation invariant diffusion, and can be used to sensitively detect changes in microstructure [20]. Recently, a diffusion model, diffusion kurtosis imaging (DKI), has been proposed as a means to quantify non-Gaussian diffusion of water within tissue microstructure [21]. This model has the advantages of simulating real living tissues in different ways. DKI can estimate the complexity of brain tissue microstructure by quantifying kurtosis index, and can obtain mean kurtosis (MK), axial kurtosis (AK) and radial kurtosis (RK) [22]. The higher the kurtosis, the more the diffusion of water molecules deviates from the Gaussian distribution, indicating that the diffusion environment is more restricted. Several studies have reported the utility of DKI in PD [23]. However, the microstructure changes of PD are diverse, which may be caused by the different degrees of disease severity. In addition, although recent studies have shown that DKI can provide additional information and even be more sensitive to changes in the microstructure of PD compared with DTI [24], the combined effects and diagnostic value of DKI and DTI parameters have not been determined.

In this study, we used the MK and FA values for early diagnosis of PD in rat models, and explored the efficacy of these values for early diagnosis of in PD rats. We aimed to construct a diagnostic model with combined application of the MK and FA value to evaluate the microstructure changes of SN in PD rats. This article is the first to propose the use of a combination of FA and MK values for early diagnosis in PD rats as well as, evaluate the diagnostic effectiveness of these combined values.

MATERIALS AND METHODS

Rat and surgery

All experiments were performed on mature (7-week-old; 200–250 g) male, Sprague-Dawley rats (n=40) (Beijing Vital River Laboratory Animal Technology Co., Ltd. China). The experiments were conducted in accordance with national guidelines for the use of experimental animals. All experimental protocols were approved by the Ethics Committee of First Hospital of Qinhuangdao (202101A141, October 17st 2021). The rats were housed in a temperature-(22 ± 2°C) and humidity-controlled (60 ± 5%) room, on a 12-h light/dark cycle, and with access to food and water ad libitum. Rats were randomly divided into two groups: (1) a PD group (n = 20) and (2) a control group (n = 20). The surgical procedures and rotation test that were used for induction and assessment of the PD model followed the published protocols by Fang *et al.*; all PD group rats were subjected to the modeling process [25].

Apomorphine-induce rotation test

All PD group rats received a single intraperitoneal injection of apomorphine (0.5 mg/kg in normal saline, Sinopharm Chemical Reagent Co., Ltd. Shanghai, China) at the beginning of every week after surgery. For rotation test, animals were allowed to habituate to the test apparatus for 10 min and then for an additional 2 min after the injection. Full rotations were counted in a cylindrical container in a dimly lit, quiet room. Rotational asymmetry was scored continuously for 30 min and then complete contralateral rotation times were scored. Rats with test scores greater than 7 were retained for the study and analysis [25].

After 6-OHDA lesion, we needed to carry out rotation test to verify the success of the animal model. At present, it was generally believed that the rat model was successfully prepared if the rotation experiment exceeded seven times per minute.

MR image acquisition and postprocessing

MR image acquisition: All 40 rats were scanned using a 3.0T Siemens TIM Verio Scanner (Siemens Medical Solutions, Erlangen, Germany) at 5 weeks after modeling. The rat head was immobilized with a custom-constructed MRI compatible rat head holder during the MR scanning. The image quality was analyzed after the MR scanning; if the rat's head moved during scanning, the scan was repeated 2 hours later with additional anesthetics. Detailed parameters of the MR sequences were as follows: 1) Axial T2WI: The MR parameters were as follows: Scan layers were aligned parallel to the anterior/posterior line with the following settings: relaxation time (TR) = 4000 msec, echo time (TE) = 113 msec, flip angle = 150, average = 6, field of view (FOV) = 80 × 80 mm, voxel size = 0.3 × 0.3 × 2.0 mm, data matrix = 192 × 192, slice thickness = 2.0 mm, and the number of slices = 10 (total scanning time = 3 minutes 18 seconds). 2) DKI: The MR parameters were as follows: Scan layers were aligned parallel to the anterior/posterior line with the following settings: TR = 2000 msec，TE = 107 msec, flip angle = 180，FOV = 144 × 144 mm, slice thickness = 2 mm, number of slices = 10, voxel size = 2.3 × 2.3 × 2 mm, data matrix = 64 × 64, sensitivity encoding (SENSE) factor = 2, 30 nonlinear directions, and b parameter

[DOI: 10.61186/ijrr.22.2.339]

of 0, 1000, and 2000 s/mm2 (total scanningtime = 11 minutes 2 seconds). MR image postprocessing and analysis: DKI diffusion data was processing via the Diffusional Kurtosis Estimator (DKE) on the MatLab 2017a platform (MathWorks, Natick, MA, Massachusetts, United States). Image J soft ware (NIH, Massachusetts, United States) was used to read, measure, and record data. The FA and MK parameter maps of the rat brains were referenced with T2WI rat brain images for the exact identification of the damaged cortex and contralateral mirrored area. Two independent radiologists with 10 years of experience in neural MRI, who were blinded to the animal grouping, placed circular regions of interest (ROIs) measuring 0.30–0.60 cm^2 in the right SN. See figure 1 for MRI.

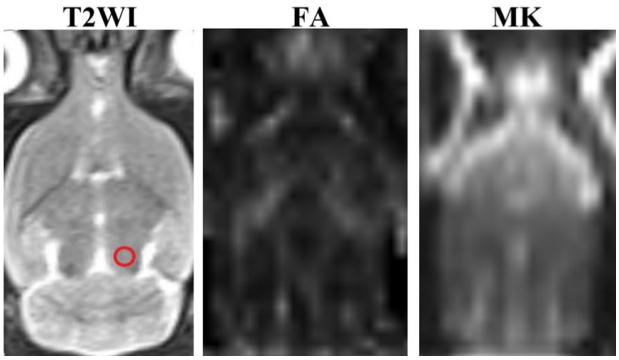

Figure 1. Figure A shows the T2WI image, the small red circle shows the ROIs, figure B shows the FA image, and figure C shows the MK image.

Immunohistochemistry and histochemistry

Forty rats were anesthetized again after MRI scans. The brains were removed, and tissues were prepared as published previously. Coronal vibrate sections were dissected from each brain and sliced into 8 μm sections through the ventral mesencephalon. The SN sections were selected for immunohistochemistry, and all the sections from different rat brains were matched as closely as possible. Immunohistochemistry for tyrosine hydroxylase (TH) was studied with reference to Fang *et al.* [25]. Tunel staining was processed by an In Situ Cell Death Detection Kit (Roche, Mannheim, Germany), as the method described before [20,21]. After treating with ethanol-acetic acid (2:1), the sections were treated with proteinase K (100 μg/mL), treated with 3% H_2O_2, permeabilized with 0.5% Triton X-100, and then treated with the Tunel reaction mixture. Streptavidin HRP working solution was added dropwise for reaction, and DAB color development was carried out, and then hematoxylin counterstaining was carried out. Nissl staining was performed using 0.1% cresyl violet acetate solution. 30 μm thick tissue slices were transferred onto gelatinated slides and air-dried at 37 °C. Slides were then rinsed twice for 5 min with PBS and deionized in H_2O for 1 min. Sections were then stained with 0.1% cresyl acetate solution for 20 min in dark. Stained sections were rinsed with deionized water twice for 5 min to remove excess stain and further differentiated by wash in 70% ethanol until desirable staining was achieved. Then, slides were dehydrated in 90% and 96% ethanol. Finally, slides were cleared with xylene 3 times for 3 min each and coverslips were mounted onto the slides using DPX mountant.

Using the Image-Pro Plus software (Media Cybernetics Inc. Maryland, United States), the number of TH, Tunel and Nissl-positive cells in a field of 100 μm ×100 μm of the cerebellar vermis was counted.

Statistical analysis

Statistical analyses were performed using SPSS (IBM, Chicago, United States) version 21.0 software. Data were presented as the mean ± SD. The significance of the difference between the two groups was evaluated using a non-paired t test. Receiver operating characterstic (ROC) curves were constructed to evaluate the diagnostic efficacy of the MK and FA values. The cut-off values for ROC analysis were chosen as the point maximizing Youden's index. MK and FA parameters were entered into multiple logistic regression models to determine AUCs for combinations of models to evaluate diagnostic performance. Pearson's correlation analysis was employed to assess the correlation of the TH, Tunel and Nissl staining density with the MRI parameters. P values < 0.05 were considered statistically significant for all analyses.

RESULTS

Comparative analysis of FA and MK values within and between groups of PD rats

There was no statistically significant difference in FA value and MK value between the two groups before modeling. At 5th week after modeling, the FA value and MK value in the PD group were higher than those in control group, and the difference was statistically significant (figure 2A). The comparison within the group showed that the FA value and MK value in PD group 5 week after the modeling were greater than those before the modeling, and the difference was statistically significant, while the control group shoeed no difference before and after the modeling. See table 1 for details.

Diagnostic efficacy test of FA value and MK value 5th week after modeling

The ROC curve was used to analyze the diagnostic efficacy of FA value and MK value. The results showed that the AUC of the FA value was 0.878 (95% confidence interval [CI]: 0.769 to 0.986), p<0.0001, the corresponding cut-off value was 0.395, sensitivity 65%, specificity 100%, and Youden's index 0.65. While the AUC of MK value was 0.901 (95% CI: 0.810

[DOI: 10.61186/ijrr.22.2.339]

to 0.993), P < 0.0001, the corresponding cut-off value was 1.085, sensitivity 75%, specificity 90%, and Youden's index 0.65.

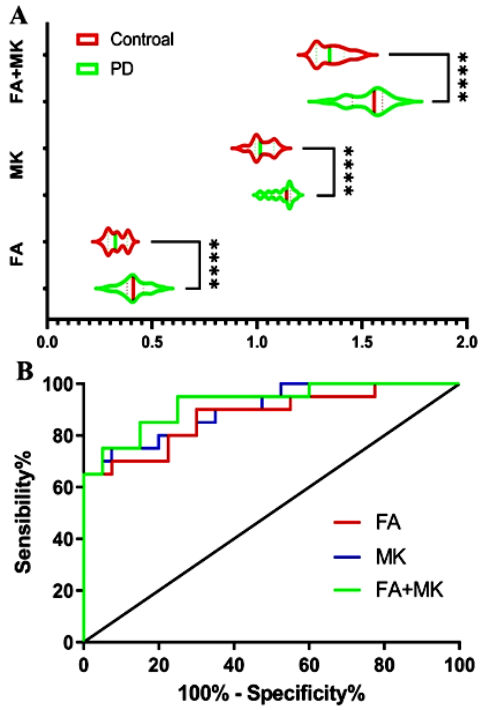

Figure 2. Figure shows that the FA, MK and FA+MK values of the PD group were significantly higher than those of the control group at the 5th week after modeling, and the difference was statistically significant **(A);** and ROC curve analysis, and the area under FA+MK curve was the largest **(B)**.

Table 1. The FA and MK values of PD rats before and after modeling surgery showed statistical differences, while the inter group comparison showed that the FA and MK values of PD group rats were significantly higher than those of the control group, and the differences were statistically significant.

group	MR parameters	Pre-surgery	After-surgery	Intra group comparison	
				t	p
PD	FA	0.332± 0.041	0.415± 0.062	4.296	0.0001*
	MK	1.046± 0.035	1.121± 0.053	4.951	<0.0001*
Control	FA	0.329± 0.030	0.330± 0.043	0.071	0.944
	MK	1.035± 0.034	1.027± 0.050	0.555	0.582
Between the two groups	FA	t=0.251 (p=0.803)	t=5.038 (p<0.0001*)	-	-
	MK	t=0.832 (p=0.411)	t=5.802 (p<0.0001*)	-	-

When FA+MK values were combined for diagnosis, FA+MK values after modeling were significantly higher than those before modeling, and the difference was statistically significant (t = 6.912, P<0.0001). At the 5th week after modeling, the FA+MK value in the PD group was significantly higher than that in control group, and the difference was statistically significant (figure 2A). ROC curve analysis showed that the AUC was 0.925 (95% CI: 0.846 to 1.000), P<0.0001, the corresponding cut-off value was 1.404, sensitivity 95%, specificity 75%, and Youden's index 0.70. The Youden's index of FA+MK combined diagnosis was higher than that of two parameters diagnosed separately (As shown in figure 2B).

TH, Tunel and Nissl staining 5th week after modeling

The results showed that the number of TH-positive cells per square millimeter in the SN of PD rats was 23.95±5.62, and that of neuronal cells (37.46±8.89)×10, which was significantly lower than that in the control group (47.30 ± 6.69) (t = 11.95, p< 0.0001), 100.23 ± 13.48 ×10 (t = 17.38, p< 0.0001). The number of apoptotic cells per square millimeter in the PD group was significantly higher than that in control group (19.80 ± 7.49 vs. 3.50 ± 1.76, t = 9.47, p< 0.0001) (As shown in figure 3A). See figure 4 for cell staining pictures.

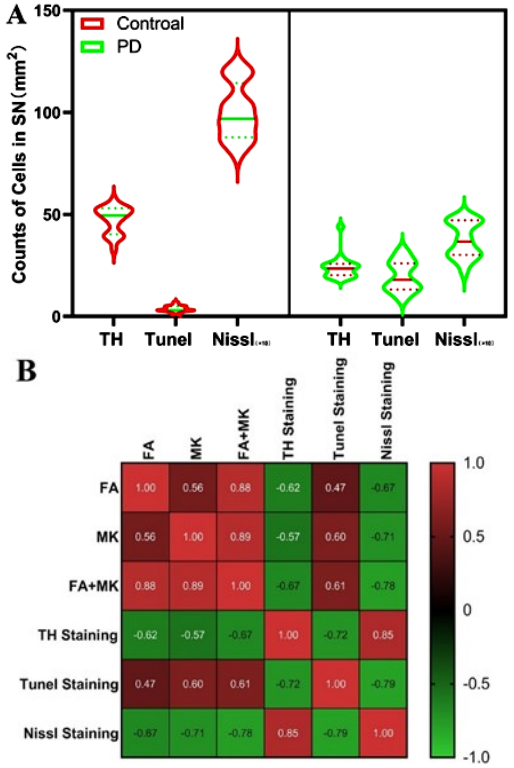

Figure 3. Figure shows that at the 5th week after modeling, the number of TH and Nissl stained positive cells in PD group was significantly lower than that in control group, while the number of Tunel stained positive cells was significantly higher than that in control group **(A)**; and correlation analysis between magnetic resonance parameters and pathological positive cells **(B)**.

Correlation analysis between magnetic resonance parameters and pathological positive cells

The results showed that FA value was negatively correlated with the number of TH and Nissl staining positive cells, but positively correlated with the number of Tunel staining positive cells. MK value was

[DOI: 10.61186/ijrr.22.2.339]

also negatively correlated with TH and Nissl staining positive cells, but positively correlated with the number of Tunel staining positive cells. However, it appears that FA value is slightly less affected by apoptotic cells than MK value, and there is no significant difference between the other two groups (figure 3B).

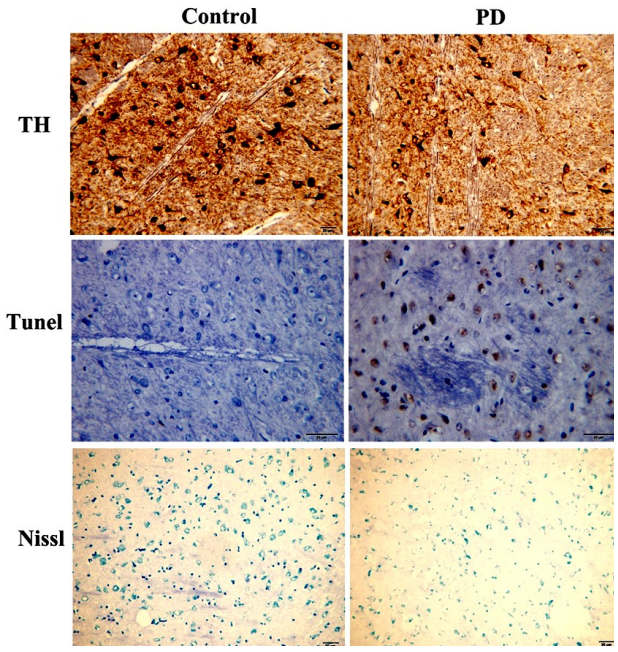

Figure 4. The top two images show that the number of TH positive cells in the SN of PD group rats is significantly higher than that of the control group. While the middle two images show that the number of Tunel positive cells in the SN of PD group rats is significantly lower than that of the control group. The bottom two images show that the number of neurons in the SN of PD rats is significantly higher than that of the control group.

DISCUSSION

In this study, we combined DKI and DTI techniques to study the microstructure changes of SN in PD rats. The main findings of this study are as follows: (1) in the PD rat group, the FA and MK values are higher 5 weeks after modeling than before modeling. (2) five weeks after modeling, both FA and MK value in the PD rat group are significantly higher than those in control group, but the AUC of the MK value is higher than that of FA value, and the AUC of the FA+ MK value is higher than of the two, and Youden's index is the highest. (3) The number of TH-positive cells and neuronal cells in the SN of PD rats is significantly lower than that in control group 5 week after modeling, while the number of Tunel-positive cells is significantly higher than that in the control group. (4) The correlation results show that FA and MK values are negatively correlated with the number of TH- and Nissl-positive cells, but positively correlated with the number of Tunel-positive cells.

The FA and MK values in the SN 5 week after modeling are higher than those before modeling, and the comparison between groups is significantly higher than that in the control group. We consider that this is related to the changes in the microstructure of the SN of PD rats after modeling [26]. Neuropathological reports indicate that dopaminergic neurons are lost in the SN of PD patients α-synuclein aggregation and glial cell infiltration are the main neuropathological changes [17,27,28]. As a part of gray matter, water diffusion in SN should be relatively isotropic [23]. Due to the neurodegeneration process in this region, the water diffusivity becomes relatively "anisotropic", and the tissue structure becomes complex, which can be manifested by the increased FA value in this study [23]. As a new diffusion model imaging method, DKI can quantify the degree of non-Gaussian water diffusion [24]. This model has the advantage of simulating real living tissue in different ways. DKI can estimate the complexity of brain tissue microstructure by quantifying kurtosis index: the higher the MK, the more the diffusion of water molecules deviates from the Gaussian distribution, indicating that the diffusion environment is more restricted [21]. Our experiment finds that the MK value after modeling is significantly higher than those before modeling and in the control group. The increase of MK may reflect the increase of water molecule diffusion disorder caused by protein accumulation, neuroinflammation or other pathology in SN of PD rats. In addition, studies have shown that: α-synuclein accumulation usually increases diffusion heterogeneity and eventually increases diffusion kurtosis values [21].

DTI mainly uses the diffusion anisotropy of water molecules and FA value characteristics of tissues to detect the microstructure characteristics of tissues [29]. The three-dimensional ellipse is taken as the axis, and the eigenvector in the second-order three-dimensional is used to describe the diffusion of water molecules and FA value [30]. DKI is a fourth-order three-dimensional fully symmetric tensor. DTI is a second-order tensor, therefore, the generation of DKI technology must undergo a transition from a second-order tensor to a fourth-order tensor. The spatial diffusion coefficient of the second-order tensor is an ellipsoid sphere. The main axis of the ellipsoid is oriented in the direction of the main eigenvector and coincides with the direction of the brain nerve fibers, while that of the secondary eigenvector is perpendicular to the direction of the fibers. The ellipsoid of the second-order tensor cannot coincide with the multi-fiber trend; therefore, DTI cannot solve the multi-fiber crossing problem. DKI compensates for the deficiency of the second-order tensor by adding a fourth-order tensor correction term to the imaging formula [31,32]. This study shows

[DOI: 10.61186/ijrr.22.2.339]

that as a non-Gaussian water diffusion model, the diagnostic efficiency of MK value is slightly higher than FA value. The size of MK value depends on the complexity of the tissue structure in ROI. The more complex the structure, the more significant the diffusion restriction of non-normally distributed water molecules, and the larger the MK value [23]. The normal diffusion in each voxel is closely related to the factors of water diffusion suggesting that it is not an anisotropic environment. Therefore, the change of MK value may be caused by different factors, such as pathological protein accumulation or iron deposition, and gliosis [26,33]. The FA value is mainly related to the integrity and direction of the fiber bundle, but the SN fiber bundle changes in PD rats are only part of the pathological changes [34]. Therefore, the diagnostic sensitivity of FA value is slightly lower than that of MK value. However, the sensitivity of the combined diagnosis of PD is significantly increased, and the diagnostic efficiency is higher than that of the combined diagnosis of PD in rats. After considering the combination of the two, they can compensate each other's limitations, which can significantly improve the diagnostic efficiency.

For the pathological results, there is a certain correlation between the MR parameters and pathological changes. Both of them are positively correlated with the number of apoptotic cells, and negatively correlated with that of TH-positive and neuronal cells. Possible reasons are as follows: (1) After the apoptosis of neurons in SN region, the nucleus of neurons shrinks, chromatin condenses into a block or crescent shape and converge, and misfolded α-synuclein, after aggregation, produces apoptotic bodies (Lewy bodies) and so on [35], while a - synuclein further aggravates neurotoxic effects through mitochondrial function damage, endoplasmic reticulum function defect, protease action, glial inflammatory reaction, cell membrane damage, lysosomal function defect and synaptic dysfunction [36]. At this time, the loss of neuronal cells leads to the damage of nerve fibers and the proliferation of glial cells, thus causing various specific manifestations of SN water molecule diffusion [26]. With the apoptosis of neurons in the SN and the accumulation of harmful substances, the local water molecule diffusion is affected, resulting in the marked increase of MK value. (2) The less apoptosis of neurons, the higher the number of TH-positive and neuronal cells, and the local microstructure still shows relatively mild changes. Therefore, the impact on FA value and MK values is small. The only difference between the two is that the correlation coefficient between MK value and Tunel is higher than that between FA value and Tunel staining, which may be related to the fact that MK value is more seriously affected by apoptotic substances, which also confirms the above inference that MK value is better than FA value.

In this study, some limitations should be noted. First, this study lacks clinical validation, and the sample size is small, which is prone to causing certain errors. Second, because the volume of SN in PD rats is so small, measurement errors may occur when obtaining MK and FA values. In conclusion, our results indicate that there are microstructural changes in the SN neurons in PD rats. DKI is sensitive to the changes in the brain microstructure in the SN of PD rats, and the combination of kurtosis and tensor can achieve a good diagnosis of PD. It has been preliminarily confirmed that the combination of FA and MK values has great value for early diagnosis of PD rats, and there is an opportunity to promote it to clinical practice in the future.

Funding: This research was supported by the Qinhuangdao Science-Technology Support Projects of China (202101A141).

Conflicts of interest statement: The authors had no conflicts of interest to declare.

Ethical consideration: All experimental protocols were approved by the Ethics Committee of First Hospital of Qinhuangdao (202101A141, October 17st 2021).

Author contributions: YS C and YC D contributed to the design of the study and the development of the study protocol, YS C and DY Acoordinated the study. YC D performed the systematic review, including data collection and data analysis. All authors contributed to data interpretation, manuscript drafting and review. YS C drafted the first version of the manuscript.

REFERENCES

1. Nachman E and Verstreken P (2022) Synaptic proteostasis in Parkinson's disease. *Curr Opin Neurobiol, **72**: 72-79*.
2. Chen J, Xu J, Huang P, *et al.* (2022) The potential applications of traditional Chinese medicine in Parkinson's disease: A new opportunity. *Biomed Pharmacother, **149**: 112866*.
3. Bloem BR, Okun MS, Klein C (2021) Parkinson's disease. *The Lancet, **397**: 2284-2303*.
4. Simonet C, Schrag A, Lees AJ, Noyce AJ (2021) The motor prodromes of parkinson's disease: from bedside observation to large-scale application. *J Neurol, **268**: 2099-2108*.
5. Qian H, Kang X, Hu J, *et al.* (2020) Reversing a model of Parkinson's disease with in situ converted nigral neurons. *Nature, **582**: 550-556*.
6. Xie L and Hu L (2022) Research progress in the early diagnosis of Parkinson's disease. *Neurol Sci, **43**(11): 6225-6231*.
7. Sun X, Liu F, Liu Q, *et al.* (2019) Quantitative research of (11)C-CFT and (18)F-FDG PET in parkinson's disease: A pilot study with NeuroQ software. *Front Neurosci, **13**: 299*.
8. Rebelo D, Oliveira F, Abrunhosa A, *et al.* (2021) A link between synaptic plasticity and reorganization of brain activity in Parkinson's disease. *Proc Natl Acad Sci, USA 118*.
9. de Souza AM, Pitombeira MS, de Souza LE, *et al.* (2021) (11)C-PK11195 plasma metabolization has the same rate in multiple sclerosis patients and healthy controls: a cross-sectional study. *Neural Regen Res, **16**: 2494-2498*.
10. Cheon M, Kim SM, Ha SW, *et al.* (2022) Diagnostic Performance for Differential Diagnosis of Atypical Parkinsonian Syndromes from Parkinson's Disease Using Quantitative Indices of (18)F-FP-CIT PET/CT. *Diagnostics, (Basel) 12*.

[DOI: 10.61186/ijrr.22.2.339]

11. Hsu SY, Lin HC, Chen TB, *et al.* (2019) Feasible classified models for parkinson disease from (99m)Tc-TRODAT-1 SPECT Imaging. *Sensors (Basel), 19*.
12. Rammohan N, Randall JW, Yadav P (2022) History of technological advancements towards MR-Linac: The future of image-guided radiotherapy. *J Clinical Medicine, **11**: 4730*.
13. Zhao XJ, Niu XY, You HY, *et al.* (2019) Signal Alteration of Substantia Nigra on 3.0T Susceptibility-weighted Imaging in Parkinson's Disease and Vascular Parkinsonism. *Curr Med Sci, **39**: 831-835*.
14. Zheng JH, Sun WH, Ma JJ, *et al.* (2022) Structural and functional abnormalities in Parkinson's disease based on voxel-based morphometry and resting-state functional magnetic resonance imaging. *Neurosci Lett, **788**: 136835*.
15. Li K, Su W, Li SH, *et al.* (2018) Resting state fMRI: A valuable tool for studying cognitive dysfunction in PD. *Parkinsons Dis, **2018**: 6278649*.
16. Kouli A, Torsney KM, Kuan WL (2018) Parkinson's disease: Etiology, neuropathology, and pathogenesis. In: Stoker TB, Greenland JC, editors. Parkinson's Disease: Pathogenesis and Clinical Aspects. Brisbane (AU).
17. Terse PS, Kells AP, Noker P, *et al.* (2020) Safety assessment of AAV2-hGDNF administered via intracerebral injection in rats for treatment of parkinson's disease. *Int J Toxicol, 1091581820966315*.
18. Hall JM, Ehgoetz Martens KA, *et al.* (2016) Diffusion alterations associated with Parkinson's disease symptomatology: A review of the literature. *Parkinsonism Relat Disord, **33**: 12-26*.
19. Zhang Y and Burock MA (2020) Diffusion tensor imaging in parkinson's disease and parkinsonian syndrome: A systematic review. *Front Neurol, **11**: 531993*.
20. Chung SJ, Cho KH, Lee YH, *et al.* (2021) Diffusion tensor imaging-based pontine damage as a degeneration marker in synucleinopathy. *J Neurosci Res, **99**: 2922-2931*.
21. Kasa LW, Haast RAM, Kuehn TK, *et al.* (2021) Evaluating High Spatial Resolution Diffusion Kurtosis Imaging at 3T: Reproducibility and Quality of Fit. *J Magn Reson Imaging, **53**: 1175-1187*.
22. Bai X, Zhou C, Guo T, *et al.* (2021) Progressive microstructural alterations in subcortical nuclei in Parkinson's disease: A diffusion magnetic resonance imaging study. *Parkinsonism Relat Disord, **88**: 82-89*.
23. Bingbing G, Yujing Z, Yanwei M, *et al.* (2020) Diffusion Kurtosis Imaging of Microstructural Changes in Gray Matter Nucleus in Parkinson Disease. *Front Neurol, **11**: 252*.
24. Arab A, Wojna-Pelczar A, Khairnar A, *et al.* (2018) Principles of diffusion kurtosis imaging and its role in early diagnosis of neurodegenerative disorders. *Brain Res Bull, **139**: 91-98*.
25. Fang Y, Dong Y, Zheng T, *et al.* (2017) Altered tracer distribution and clearance in the extracellular space of the substantia Nigra in a rodent model of parkinson's disease. *Front Neurosci, **11**: 409*.
26. Dong Y, Liu D, Zhao Y, *et al.* (2021) Assessment of neuroprotective effects of low-intensity transcranial ultrasound stimulation in a parkinson's disease rat model by fractional anisotropy and relaxation time T2(*) value. *Front Neurosci, **15**: 590354*.
27. Wei X, He S, Wang Z, *et al.* (2014) Fibroblast growth factor 1attenuates 6-hydroxydopamine-induced neurotoxicity: an *in-vitro* and *in-vivo* investigation in experimental models of parkinson's disease. *Am J Transl Res, **6**: 664-677*.
28. Sy MAC and Fernandez HH (2020) Pharmacological treatment of early motor manifestations of parkinson disease (PD). Neurotherapeutics.
29. Ikenouchi Y, Kamagata K, Andica C, *et al.* (2020) Evaluation of white matter microstructure in patients with Parkinson's disease using microscopic fractional anisotropy. *Neuroradiology, **62**: 197-203*.
30. Wu EX and Cheung MM (2010) MR diffusion kurtosis imaging for neural tissue characterization. *NMR Biomed, **23**: 836-848*.
31. Han D, Qi L, Wu EX (2008) Extreme diffusion values for non-Gaussian diffusions. *Optimization Methods and Software, **23**: 703-716*.
32. Qi L, Han D, Wu EX (2009) Principal invariants and inherent parameters of diffusion kurtosis tensors. *J Mathematical Analysis and Applications, **349**: 165-180*.
33. Dong Y, Yuan Y, Fang Y, *et al.* (2020) Effect of aquaporin 4 protein overexpression in nigrostriatal system on development of Parkinson's disease. *Int J Neurosci, 1-8*.
34. Khairnar A, Ruda-Kucerova J, Arab A, *et al.* (2021) Diffusion kurtosis imaging detects the time-dependent progress of pathological changes in the oral rotenone mouse model of Parkinson's disease. *J Neurochem, **158**: 779-797*.
35. Zhao X, He H, Xiong X, *et al.* (2022) Lewy Body-Associated Proteins A-Synuclein (a-syn) as a Plasma-Based Biomarker for Parkinson's Disease. *Front Aging Neurosci, **14**: 869797*.
36. Chen V and Saez-Atienzar S (2018) A tango for two: Dopamine and alpha-synuclein synergy may explain nigrostriatal degeneration in Parkinson's disease. *Mov Disord, **33**: 249*.

[DOI: 10.61186/ijrr.22.2.339]